ACADEMIC PRESS

Available online at www.sciencedirect.com
SCIENCE DIRECT®

Journal of Catalysis 213 (2003) 23–38

JOURNAL OF CATALYSIS

www.elsevier.com/locate/jcat

A C1 mechanism for methane oxidation on platinum

P. Aghalayam,[a] Y.K. Park,[a] N. Fernandes,[a] V. Papavassiliou,[b]
A.B. Mhadeshwar,[c] and D.G. Vlachos [c,*]

[a] *Department of Chemical Engineering, University of Massachusetts—Amherst, Amherst, MA 01003-3110, USA*
[b] *Praxair Technology Center, 175 East Park Dr., Tonawanda, NY 14151, USA*
[c] *Department of Chemical Engineering and Center for Catalytic Science and Technology (CCST), University of Delaware, Newark, DE 19716-3110, USA*

Received 27 February 2002; revised 3 September 2002; accepted 13 September 2002

Abstract

Platinum-catalyzed methane oxidation processes have significant potential in pollutant emission control and chemical synthesis. Detailed models, including elementary gas and catalyst phase chemistry and multicomponent transport, have been developed in the literature. However, the catalyst-phase chemical reaction mechanisms have a number of drawbacks. In this study, we apply a multistep methodology to construct a C1 surface reaction mechanism for methane oxidation on platinum. First, a comprehensive set of elementary C1 reaction steps is laid down, followed by calculation of thermodynamically consistent, species-coverage-dependent activation energies and heats of reaction. Next, order-of-magnitude estimates of the preexponentials are obtained from transition state theory and simulations are conducted using this reaction mechanism to obtain predictions of targeted experiments. Reaction path analysis and sensitivity analysis are subsequently employed to identify the important steps for each experiment and refine the preexponentials of these reactions. Finally, this mechanism is validated by comparison with other sets of experiments. Ignition and extinction temperatures, fuel conversion, selectivity to syngas, and laser-induced fluorescence signals from OH radicals, under various operating conditions, are predicted well by the mechanism. It is found that the dominant pathway for the surface dissociation of methane changes with operating conditions from oxygen-assisted prior to ignition to pyrolytic at high temperatures and for fuel-rich mixtures. A coupling between the carbon and hydrogen subsets of the reaction mechanism is identified through analysis of the hydroxyl mole fraction at high temperatures. Overall, this surface reaction mechanism overcomes many limitations of previous work and is capable of capturing the physics of methane oxidation on platinum over a wide range of operating conditions.

Keywords: Microkinetic analysis; Thermodynamic consistency; Catalytic partial oxidation; Mechanism development; Methane; Syngas; Hydrogen; Optimization

1. Introduction

The complete and partial oxidation of methane over noble metal catalysts has received much attention because methane is the main constituent of natural gas, which is an abundant and cheap feedstock. Natural gas can be used for energy production, chemical synthesis, and hydrogen production for fuel cell applications. Energy production may be accomplished homogeneously or catalytically. The latter is an efficient energy production process with relatively low pollutant emissions [1,2] compared to the former. However, commercialization of catalytic combustion has been hindered by a lack of fundamental understanding of the underlying microprocesses. In addition, direct partial oxidation of methane over platinum and rhodium catalysts in short-contact-time monoliths presents a promising alternative to steam reforming for the production of synthesis gas, an important intermediate in chemical synthesis [3–5]. Production of synthesis gas from methane with Ni catalysts in a fluidized bed reactor at elevated temperatures and pressures has also been demonstrated [6]. Recent reviews on partial oxidation are given in [5,7,8].

Earlier modeling of methane oxidation on platinum used one-step or simplified chemistry models to describe the surface reactions [9,10]. Due to a change in the rate-limiting step with temperature and/or composition in most catalytic oxidation systems [11], detailed surface reaction mechanisms for methane oxidation are essential to capture the underlying physics and develop predictive models for

* Corresponding author.
E-mail address: vlachos@ecs.umass.edu (D.G. Vlachos).

0021-9517/03/$ – see front matter
PII: S0021-9517(02)00045-3

reactor design. Towards this goal, several surface reaction mechanisms for methane oxidation on platinum have been proposed in the literature [12–17]. These mechanisms use many kinetic parameters obtained from independent surface science experiments. The rest of the kinetic parameters have been tuned to fit either ignition in stagnation geometry [12,15] or the conversion and selectivities of fuel-rich mixtures [13,14]. The mechanism of [16] gives reasonable predictions for bifurcation and selectivity, whereas that of [17] was developed for ethane oxidation on platinum. Although significant advances in our understanding has been achieved from these mechanisms, they generally have some inherent drawbacks that preclude their use as comprehensive mechanisms capable of predicting all experimental data. These limitations have been elaborated on in [16,18,19].

In brief, we have found that these mechanisms are incapable of simultaneously predicting ignition temperature and syngas selectivity data. In addition, the predicted extinction temperatures are often lower than the ignition temperatures, in contrast to experimental data. Furthermore, it is difficult to maintain thermodynamic consistency in energetics of large surface reaction mechanisms and to account for adsorbate–adsorbate interactions in the activation energies of all surface reactions (which is necessary in order to maintain thermodynamic consistency in energetics). Finally, none of these mechanisms considers a comprehensive set of elementary reaction paths on the surface. The implications of these limitations for reactor design and scaleup are significant. For example, the premature ignition predicted in [16] using the Hickman and Schmidt mechanism results in poor prediction of hot spots and diminishes the chance for contribution of gas-phase reactions, which can be important at high pressures. This indicates the need for a surface reaction mechanism with elementary-like reactions, which can help to extrapolate models to conditions for which no experimental data are available and to handle multiple paths for selectivity and pollutants prediction.

We have recently proposed a multistep methodology for the construction of thermodynamically consistent, detailed surface reaction mechanisms, with coverage-dependent kinetic parameters. The mechanisms were mathematically optimized against multiple sets of experimental data. Successful application of this methodology to both hydrogen and carbon monoxide oxidation on Pt was demonstrated, and the mechanisms were extensively validated through comparison of predictions against additional (redundant) experiments over a wide range of operating conditions [18–20]. In this paper we apply elements of this methodology to develop a C1 reaction mechanism for methane oxidation over Pt, which overcomes several limitations of earlier mechanisms and is applicable over a wide range of operating conditions. The emphasis of this paper is on the development of a reaction mechanism rather than sophisticated reactor scale models, and therefore, we choose to analyze experiments where simpler transport is adequate or to draw only semiquantitative comparisons with experiments whose transport models are complicated. The proposed mechanism can be considered an initial screening one, with rigorous mathematical optimization of some of the parameters illustrated at the end of the paper.

2. Overview of experimental data

Several experiments on methane oxidation have been conducted that are valuable in mechanism development or reactor design for a variety of reasons. A necessary first step in either complete or partial oxidation is catalyst ignition. Furthermore, ignition, extinction, and autothermal temperatures delimit reactor operation regimes [21]. Thus, it is important to be able to model and understand these bifurcation characteristics of methane in order to operate both combustion and partial oxidation processes safely and efficiently. Upon ignition, the conversion of methane, the selectivity to various partial oxidation products, the energy efficiency, and pollutant emissions are important optimization targets for chemical synthesis and complete combustion. In particular, as the new process of syngas production from the direct partial oxidation of fuel-rich methane/oxygen mixtures is explored, models to capture the experimental trends, including fuel conversion and product selectivity, are vital. Similar information is essential for catalytic combustion as well. Prediction of OH radical concentration at high temperatures is important to understand the coupling between gas and surface-phase chemistries, the latter being important in selectivities and reactor safety. Furthermore, we have found in earlier work on surface reaction mechanism development that species concentrations are very sensitive to surface reactions, and not merely to adsorption steps. In particular, predicting the experimentally measured OH radical concentration has been crucial to the optimization of the H_2/O_2 mechanism [18,19]. Below, we present selected experimental data that are used either for mechanism development (targeted experiments) or validation (redundant experiments).

2.1. Bifurcation characteristics

Figure 1 compiles experimentally measured ignition temperatures of methane versus a normalized inlet composition, from different groups [22–24]. The experiments of [22,24] have been performed using a Pt foil, with 94% nitrogen-diluted methane–oxygen mixtures and methane–air mixtures, respectively. Griffin and Pfefferle, on the other hand, have used a platinum wire, with 25% nitrogen dilution of the total reactant flow [23]. Experiments conducted in our laboratory are also indicated in this figure, for a 94% nitrogen dilution case and mixtures of methane in air [25].

The ignition temperature is seen to decrease with increasing inlet methane composition; i.e., the fuel has a promoting influence on ignition. It is interesting to note that although different dilution levels, flow rates, and reactor geometries have been used in these experiments, ignition temperatures

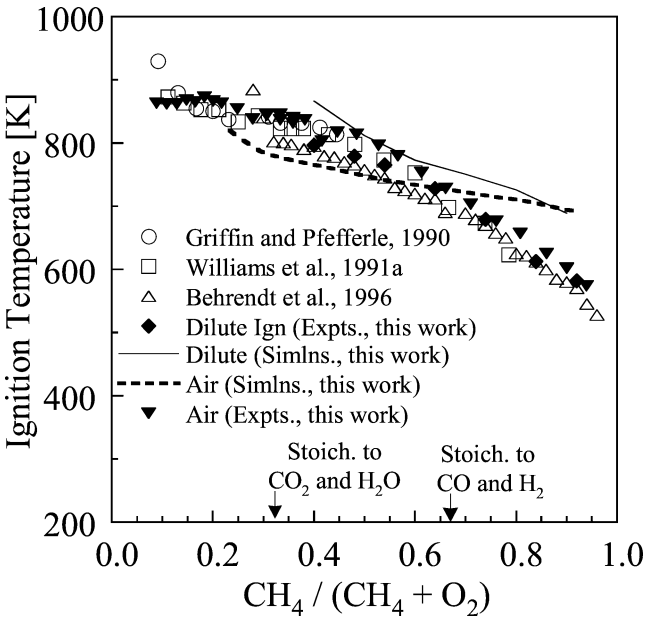

Fig. 1. Ignition temperature as a function of the inlet fuel/oxygen ratio. Experimental data are shown in symbols and model predictions in lines. The inlet compositions corresponding to the stoichiometric one for complete and partial oxidation are indicated by arrows. Ignition temperature is insensitive to dilution, catalyst form, and flow rate over a range of conditions. The model predictions are in good agreement with the experiments. The simulations have been performed using a strain rate of 5 s^{-1}, a convective heat loss factor from the back of the catalyst surface of 10^{-4} cal/cm^2/s, and a radiative surface emissivity of 0.15 at a pressure of 1 atm and an inlet temperature of 25 °C.

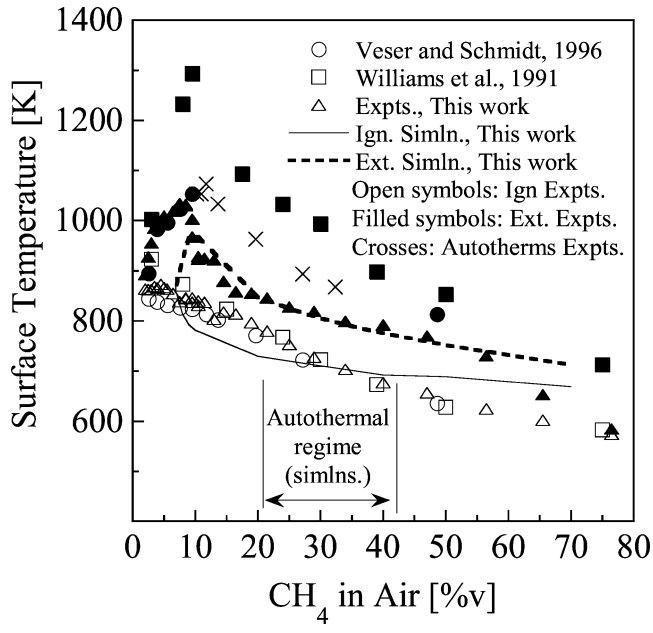

Fig. 2. Experimental ignition (open symbols), extinction (filled symbols), and autothermal (crosses) temperatures and model predictions (lines) as a function of the inlet fuel composition in air. The extinction temperature is higher than the ignition one in all cases but it is quite sensitive to the experimental setup. A maximum in extinction temperature around the stoichiometric is observed. Overall, good agreement between experiments and predictions is found. The conditions for the simulations are the same as in Fig. 1.

at a fixed relative methane/oxygen ratio do not vary much. We have previously suggested that such an insensitivity of ignition temperature on dilution and reactor geometry indicates that ignition is primarily governed by the kinetics of the oxidation process rather than, for example, reaction exothermicity [26], which is the classical mechanism for reactor multiplicity. This behavior is in contrast to homogeneous ignition of methane, where dilution and thermal effects play an important role [27,28]. Such behavior indicates that adsorption of reactants has to be competitive, in agreement with previous sensitivity analysis [12]. We propose that straightforward experiments of varying dilution can delineate the mechanism inducing ignition, i.e., thermal feedback versus competitive adsorption of reactants. Since it is not clear from the literature experimental data whether the terminal point (a cusp point in bifurcation theory) of the fuel-lean side was determined by the differences in the experimental setup and operating conditions, we have conducted CH_4/air and diluted CH_4/O_2 experiments in our stagnation flow reactor, described in detail in [29]. We have found that indeed the cusp point shifts to higher CH_4 compositions with increasing dilution, whereas the ignition temperature does not strongly depend on dilution. We attribute this shift of the cusp point to extinction, which we have previously found to be thermally controlled.

Even though many studies have focused on catalytic ignition, complete bifurcation diagrams are scarce. The symbols in Fig. 2 show the ignition, extinction, and autothermal points from the experiments of [24,30] and earlier work in our group [25] for methane–air mixtures. The extinction temperature is always higher than the ignition one. Furthermore, the extinction temperatures on the fuel-lean side are higher than the ones on the fuel-rich side. No autothermal behavior has been observed in our foil experiments as compared to "pseudo-transient" autotherms seen before [30]. Some differences between the different groups, especially at the fuel-lean limit of ignition/extinction behavior, are observed. In contrast to ignition, discussed above, extinction temperatures are sensitive to the experimental setup and operating conditions. This behavior is expected as extinction is strongly affected by heat effects. We believe that the diminished heat losses from a monolith compared to a foil are mainly responsible for the presence of autothermal operation in the short contact time reactors such those of [3].

2.2. Conversion of methane and selectivity to various products

The economically viable conversion of natural gas to syngas and liquid fuels is a long-studied problem. A breakthrough in this direction is the introduction of short-contact-time microreactors for syngas production, giving high methane conversion and syngas selectivity. For example, in monolithic reactors of alumina coated with Pt, operated at millisecond contact times [3,4], conversion of methane in

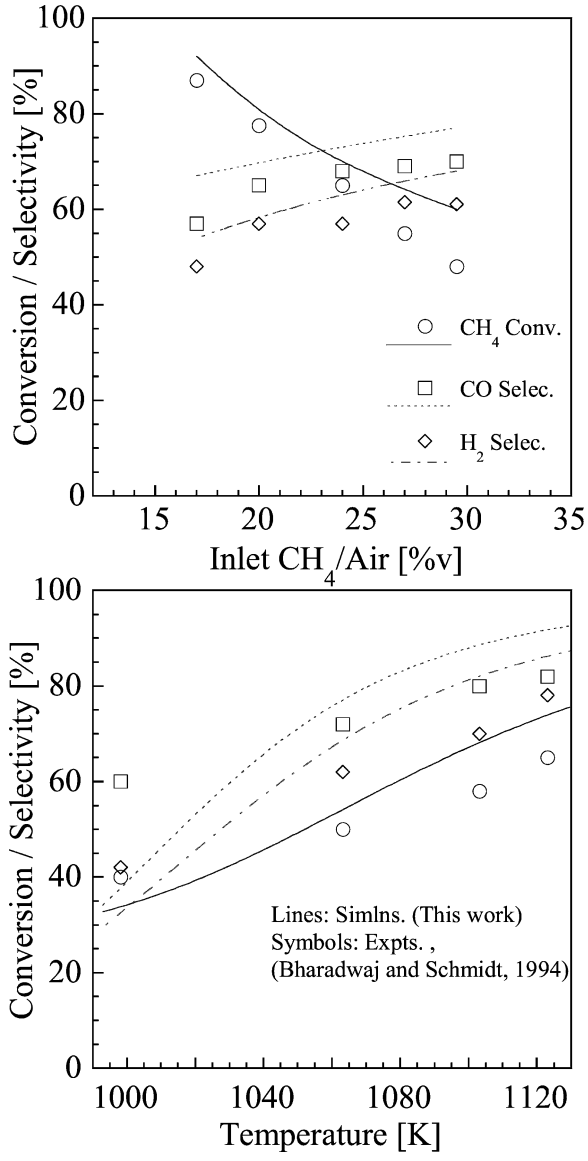

Fig. 3. Experimental data ([31]; symbols) and predicted (lines) for methane conversion and syngas selectivity as a function of inlet fuel composition (top) and temperature (bottom). The experiments have been conducted in a fluidized bed and the simulations using a catalytic CSTR, with an area-to-volume ratio of 1.5×10^4 cm^{-1} and a residence time of 0.18 s. The methane conversion decreases, whereas the selectivities to CO and H_2 increase with increasing inlet fuel composition. At a fixed inlet composition of 29.5% CH_4 in air, an increase in the operating temperature enhances conversion and selectivities (bottom). Overall, the agreement between experiments and predictions is reasonable, except for an underprediction of the CO selectivity at lower temperatures.

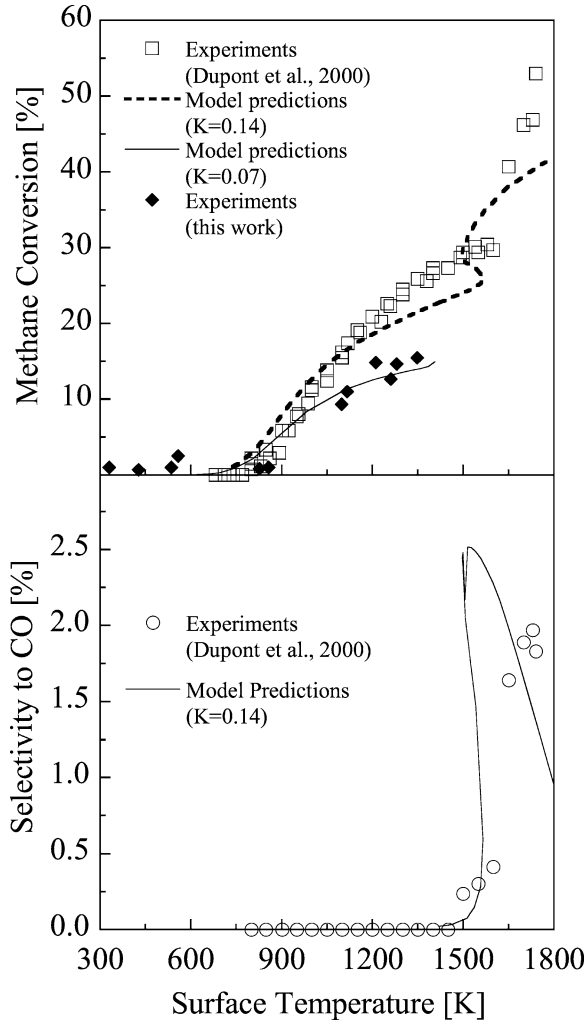

Fig. 4. Methane conversion (top) and selectivity to CO (bottom) as a function of surface temperature. Experimental data of [33], with 3.78% CH_4, 8.83% O_2, and the rest N_2 (open symbols), and this work at 6% CH_4/air (diamonds), and model predictions in lines. The methane conversion is low up to 800 K. A discontinuity in the methane conversion is observed at $\sim$ 1600 K, indicative of gas-phase reaction ignition. Good agreement between experiments and model predictions is observed.

excess of 60%, with CO and H_2 selectivities greater than 80 and 50%, respectively, were measured. In a fluidized bed reactor (with Pt-coated Al_2O_3 beads) with a contact time of 0.1–0.5 s, selectivities and conversions were measured as functions of both operating temperature and inlet CH_4/air composition [31]. These results are shown in Fig. 3.

Similar information is needed under fuel-lean conditions for catalytic combustion studies, but such data had until recently been available for a packed bed only [32]. Measurements of conversion of methane and selectivity to CO using a Pt foil in a stagnation flow configuration have recently been carried out [33]. These experimental data are indicated in Fig. 4. For inlet methane compositions (at fixed nitrogen dilution) from 1.26 to 3.78%, the experiments showed a lack of dependence of methane conversion on inlet composition, up to high temperatures (1800 K). Data obtained in our laboratory, depicted also in the same figure, at an inlet methane composition of 6% in air, show lower conversions than those of Dupont et al. There are slight differences in inlet flow velocity (Dupont et al. used 8 cm/s vs 2.5 cm/s of ours) and size of catalyst foil (1.3×1.3 cm^2 vs 2×1 cm^2 of ours) in these two experiments, which could be part of the reason for the differences in methane conversion.

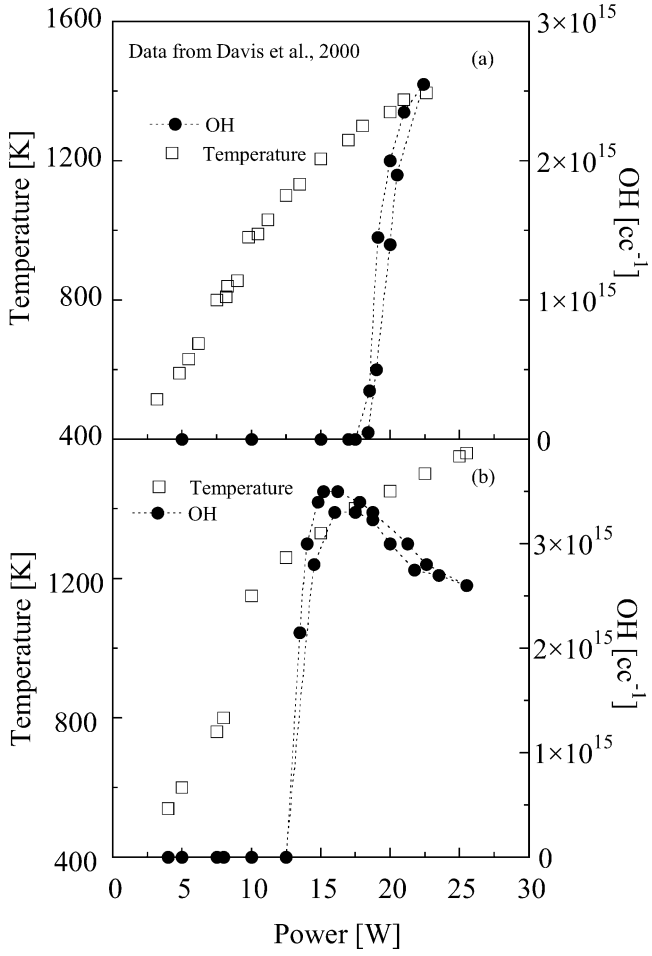

Fig. 5. Experimental data (from [38]) of surface temperature and OH concentration versus input power for 3.25% inlet CH_4/air (panel a) and 4.5% inlet CH_4/air (panel b). Hysteresis in surface temperature and a maximum in the OH concentration versus power are observed, at 4.5% CH_4/air.

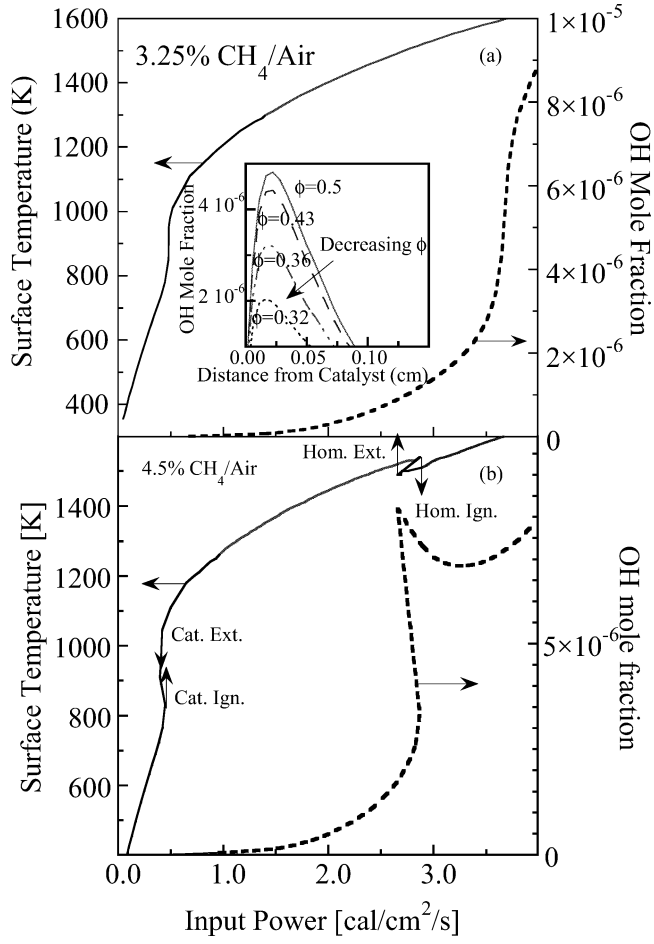

Fig. 6. Model predictions of the surface temperature and the OH mole fraction versus input power supplied to the surface for 3.25% inlet CH_4/air (panel a) and 4.5% inlet CH_4/air (panel b). For very lean mixtures, the temperature and OH mole fraction increase monotonically with the input power supplied. For richer mixtures, double hysteresis is observed at $\sim$ 800 K and $\sim$ 1500 K. The corresponding OH mole fraction exhibits a maximum. The inset in panel a shows the OH mole fraction profiles at varying inlet fuel compositions and a fixed surface temperature of 1400 K. A maximum in the OH mole fraction at $\sim$ 0.04 cm from the catalyst surface is observed in all cases. Good qualitative agreement with experiments shown in Fig. 5 may be seen. The simulations have been performed using a strain rate of 50 s^{-1} at a pressure of 1 atm and an inlet temperature of 25 °C.

2.3. Laser-induced fluorescence

Earlier laser-induced fluorescence (LIF) measurements of OH concentration have been performed at fuel-lean methane conditions at subatmospheric pressures [34] in a flat, horizontal Pt plate configuration. Modeling of such experiments is possible and has been attempted previously [35]. While this type of data are quite useful for surface mechanism development, their inherent two-dimensional nature requires complex transport models with careful evaluation of the boundary layer approximation [36,37] and potential use of elliptic formulation of the governing equations that fall beyond the scope of this investigation.

In a recent paper Schmidt and co-workers have performed experiments using Pt, Pt–Rh, and Ni gauzes, with fuel-lean methane/air mixtures, up to high temperatures (1800 K) [38]. Measurement of the temperature and the hydroxyl radical concentration using LIF near the gauze and over the spatial domain from the gauze to the fuel inlet (along the centerline of the fuel injection nozzle), were reported and are shown in Fig. 5. Corresponding model predictions, which will be discussed below, are shown in Fig. 6.

3. Development of a detailed C1 surface reaction mechanism

In brief, the steps in our methodology for detailed surface reaction mechanism development are as follows (for more details see [18]). First, a comprehensive set of elementary reaction steps are considered, based on surface science knowledge about the reaction and analogy to gas-phase reaction mechanisms, where considerable progress has been made for many important systems. Second, recourse to theory (for

example, the semiempirical unity bond index-quadratic exponential potential (UBI-QEP), known also as the bond-order conservation (BOC) method of [39]), density functional theory (DFT), or experiments (microcalorimetry) has to be made to determine heats of chemisorption for all the species that are presumed to be present on the surface, as a function of surface coverage. Using this information as an input, UBI-QEP makes possible the computation of thermodynamically consistent, coverage-dependent activation energies and heats for all the proposed reactions, through analytical equations. Third, transition state theory, literature experiments, or information from previously derived submechanisms is used to determine estimates of preexponentials and sticking coefficients of various surface reactions. Here, we have used the surface reaction steps of the H_2/O_2 submechanism from our earlier work [18] as an initial set. Transition state theory [40] is used for initial estimates of preexponentials (e.g., 10^{13} s^{-1} for desorption steps and 10^{11} s^{-1} for Langmuir–Hinshelwood type bimolecular reactions). The UBI-QEP formalism and preexponential factors are employed as a satellite to various reactor-scale codes in order to compute surface coverages, reaction rates, gaseous concentrations, and reaction energetics as the surface coverages change on the fly in a simulation. Feature identification using sensitivity, reaction path, and principal component analyses may then be used to determine the important (often termed as active parameters) preexponentials/sticking coefficients for each set of targeted experiments. Next, a mathematically rigorous optimization may be performed in order to determine the optimum values of these important preexponentials. Finally, using this optimized mechanism, comparisons with additional experimental data at other conditions have to be performed as a means of validation of the optimized mechanism.

Finally, we should remark about the complexity of modeling chemistry on realistic catalysts, such as supported or polycrystalline ones, given input data on single crystals (often on Pt(111) or Pt(100)). For many reactions, the low-index crystallographic planes are the most relevant in terms of overall reactivity. However, in real systems multiple sites exist (this is also true even for single crystals given the presence of defects), and thus, the parameters measured or predicted may be considered as some kind of ensemble average of the same elementary step on multiple sites. In that regard, the reported parameters do not actually reflect a single elementary step in the same manner as for gas-phase reactions. For this reason we prefer to input heats of chemisorption into UBI-QEP from realistic catalysts whenever possible. The thermodynamic consistency in our surface reaction mechanism is related to energetics, i.e., heats of adsorptions and activation energies. We prefer to refine crude estimates of preexponentials to account for the inherent uncertainty associated with multiple sites on the actual catalyst, and therefore, our preexponential factors represent again some kind of average of entropic contribution without an attempt to ensure thermodynamic consistency at the free energy level.

3.1. Reaction steps in methane oxidation on Pt

We lay down the elementary steps for methane oxidation on Pt based on the gas-phase methane oxidation mechanism and information from surface science experiments. In particular, the GRI 1.2 mechanism [41], which has been validated for many conditions, has first been used to deduce most reaction steps. In addition, considerable work has already been devoted to the modeling of related surface reaction systems, such as methanol synthesis from methane [42], methanol oxidation [43], CO_2 reforming of methane [44], and Fischer–Tropsch synthesis [45], to name a few. A fairly extensive set of methane reactions has been given in [42,46], where comparison of activation energies for surface reactions on various metallic catalysts has been provided, along with comparisons with experimental data whenever available.

For the purpose of presentation the reactions of methane oxidation are divided into the following classes:

(1) Adsorption and desorption of reactants, CH_4 and O_2, of the main products, CO, CO_2, H_2, H_2O, of intermediate species including H, O, OH, HO_2, H_2O_2, CH_3, CH_2, CH, C, and of various oxygenated and C2 species.
(2) Pyrolytic hydrogen abstraction from CH_x species.
(3) Oxygen-assisted and hydroxyl-assisted hydrogen abstraction from CH_x species.
(4) Reactions of O and H to form OH, HO_2, H_2O, and H_2O_2, and their interconversions (the H_2/O_2 subset).
(5) Reactions for formation of CO and CO_2 from various carbon and oxygen moieties on the surface.
(6) Formation and interconversions of oxygenated and C2 species.
(7) Reactions of oxygenated and C2 species to form products CO and CO_2.

In our current analysis, we leave the oxygenated and C2 pathways (classes 6 and 7) out because of inadequate knowledge about heats of adsorptions and the absence of significant amounts of C2 species at ignition and short-contact-time chemical synthesis conditions (which constitute our main targeted experiments). So here we have chosen to put together only a C1 mechanism. Initial calculations including the HO_2 and H_2O_2 pathways for the H_2/O_2 subset have revealed that the presence of these species in the surface reaction mechanism has slight influence on the predictions of LIF measured OH mole fractions up to considerably high temperatures. Therefore, for the sake of simplicity these species have also been left out.

3.2. Calculation of reaction energetics

An important constituent of our methodology is the input to the UBI-QEP formulation, i.e., the heats of adsorption of surface species tabulated in Table 1. It is worth noting that these numbers can be obtained for various Pt crystal surfaces from a variety of sources ranging from experiments, to

Table 1
Heat of chemisorption data

Species	Heat of adsorption (kcal/mol)	Reference
H	60.2[a]	[64]
	54.3	[43]
O	92.6[a]	[64]
C	150[a]	[64]
CH	97[a]	[45]
CH_2	68[a]	[45]
CH_3	38[a]	[45]
CH_4	6[a]	[45]
OH	60	[47]
	52.7	[43]
	63[a]	[19]
H_2O	10[a]	[45]
	10.6	[43]
CO	34[a]	[45]
	44.2	[43]

All the numbers are for Pt(111) except for OH where data are for polycrystalline Pt. Note that [47,64] report numbers calculated using UBI-QEP method, [43] reports DFT calculated numbers, and [64] reports experimental numbers.

[a] Indicates the numbers that have been used in this paper.

semiempirical theoretical calculations, to density functional theory (DFT) computations. In particular, the atomic heats of chemisorption for H, O, and C are obtained from experiments [45] or DFT calculations [43] on Pt(111) surfaces. The molecular heats of chemisorption are obtained using UBI-QEP calculations [42,45,47], using DFT calculations [43] (all on Pt(111)), and as an average of experimental values for polycrystalline Pt (e.g., the OH heat of chemisorption [19]). Finally, we must mention here that the heats of adsorption and coverage dependencies chosen here for the H_2/O_2 submechanism are identical to those in our earlier papers [18,19]. For the rest of the species, the values chosen here are indicated in Table 1.

For the C1 species considered here, there has been some direct/indirect experimental measurement of heats of adsorptions (see [18,19,46] for comparison of experiments and calculations), which are the most crucial input to UBI-QEP in calculating reaction energetics. For example, considerable work on the heat of adsorption of OH on Pt [47], along with its dependence on the surface coverage of oxygen enabled the construction of a reliable H_2/O_2 mechanism on Pt [19], which is valid over a wide range of operating conditions.

Adsorbate–adsorbate interactions strongly affect reaction energetics [19] and it is desirable to include them. Within the BOC framework, the surface coverage effect may be considered for all surface reactions (activation energies are in fact a nonlinear function of surface coverage) and not just for desorption steps as has traditionally been considered. To achieve this, adsorbate–adsorbate interactions should be included for all pairs of species; here, we prefer to include the known interactions and consider other pairs in future work. The adsorbate-adsorbate interactions chosen in our study are H–H of 6 kcal/mol, O–O of 32 kcal/mol, OH–O of 33 kcal/mol, and CO–CO of 15 kcal/mol (see our earlier papers [19,20] for discussion of these numbers). OH forms H-bonds on Pt surfaces and this effect is also taken into consideration in our BOC calculations in terms of attractive interactions. Using these numbers as input, indicated in Table 1, the UBI-QEP equations could be applied to determine the activation energies of the various reaction steps. The calculated numbers for two cases of vacancy and oxygen-dominated situations are shown in Table 2. These two cases are considered only as illustrating the important role of coverage effects and hold approximately after ignition and prior to ignition, respectively. However, given the pairs of interactions above, the activation energies can very significantly from the ones shown in Table 2, depending on the specific values of coverages.

3.2.1. Pyrolytic vs oxygen-assisted paths

Most previous mechanisms have assumed that methane decomposes in a single step, i.e., $CH_4 + 5^* \rightarrow C^* + 4H^*$. Obviously, this step cannot be elementary. UBI-QEP indicates that the oxygen-assisted path for methane decomposition has lower activation energies than the pyrolytic path for Pt, Rh, but not Ni (see [44] and Tables 2 and 3). This implies that, especially under conditions of higher oxygen coverage on the surface (i.e., moderate temperatures, oxygen-rich, and slightly reactive situations prior to ignition), the oxygen-assisted methane dissociation may be dominant over pyrolytic steps for Pt and Rh. Here we discuss this issue in more detail.

Au and Wang [48] have conducted a series of experiments on Rh/SiO_2 catalysts. Reduced and oxidized Rh catalysts have been compared in pulse and continuous flow experiments, with both CH_4 and CH_4/O_2 inputs to the system. They have found that with an oxidized catalyst, in the first pulse, the conversion of methane was higher than on a reduced one, especially at the lower temperatures (600 °C). These experiments indicated that methane dissociation could occur through both pyrolytic and oxygen-assisted paths on Rh. In contrast, in related studies over Ni, the methane conversion decreased when an oxidized catalyst was used [49,50], as compared to a reduced one. This indicates that on Ni, the oxygen-assisted path may not make a significant contribution to methane dissociation; i.e., the pyrolytic path is always the dominant one.

We have recently conducted transient experiments using a Pt-foil in stagnation flow, (see Fig. 7, taken from [25]). The foil was resistively heated to a high temperature (> 1000 K) in flows of various gas mixtures. In each experiment, the flow velocity and the power provided to the Pt foil were kept constant. The conditions are those reported in previous experiments [29]. A control run with inert N_2 indicated no variation of the temperature with time. When a small fraction of CH_4 was added to the inlet, a decrease in the foil temperature was seen due to the decomposition of CH_4 to form high emissivity carbon on the surface that in turn increases heat losses from the foil through radiation. Next, a

Table 2
Surface reaction mechanism for oxidation of methane on polycrystalline Pt

No.	Reaction	k_f	E_f $\theta_* = 1$	E_f $\theta_{O^*} = 1$	k_b	E_b $\theta_* = 1$	E_b $\theta_{O^*} = 1$
1	$OH^* + * \leftrightarrow H^* + O^*$	5.60×10^{11}	24.4	18.3	1.70×10^{10}	12.1	13.4
2	$H_2O^* + * \leftrightarrow H^* + OH^*$	1.20×10^{10}	18.4	39.1	3.50×10^{11}	12.4	0.0
3	$H_2O^* + O^* \leftrightarrow 2OH^*$	1.00×10^{11}	12.6	34.1	1.00×10^{11}	18.9	0.0
4	$H_2 + 2^* \leftrightarrow 2H^*$	0.25	0.0	0.0	1.00×10^{13}	20.0	20.0
		0.09 [c]			3.33×10^{12} [c]		
5	$O_2 + 2^* \leftrightarrow 2O^*$	0.03 [a]	0.0	0.0	1.00×10^{13} [a]	51.0	19.0
6	$H_2O + * \leftrightarrow H_2O^*$	0.70	0.0	0.0	1.00×10^{13}	10.0	10.0
		1.00 [c]			5.33×10^{12} [c]		
7	$OH + * \leftrightarrow OH^*$	1.00	0.0	0.0	1.00×10^{13}	63.0	30.0
8	$H + * \leftrightarrow H^*$	1.00	0.0	0.0	1.00×10^{13}	60.2	60.2
9	$O + * \leftrightarrow O^*$	1.00	0.0	0.0	1.00×10^{13}	92.6	67.0
10	$CH_4 + 2^* \leftrightarrow CH_3^* + H^*$	1.00 [a,b]	12.0	12.0	1.00×10^{11}	5.5	5.5
		0.68 [c]			3.97×10^{10} [c]		
11	$CH_3^* + * \leftrightarrow CH_2^* + H^*$	5.00×10^{12} [b]	25.8	25.8	1.00×10^{11}	6.1	6.1
		1.32×10^{13} [c]			4.04×10^{10} [c]		
12	$CH_2^* + * \leftrightarrow CH^* + H^*$	1.00×10^{11}	25.0	25.0	1.00×10^{11}	12.2	12.2
13	$CH^* + * \leftrightarrow C^* + H^*$	1.00×10^{11}	5.4	5.4	1.00×10^{11}	37.6	37.6
14	$CH_3^* + O^* \leftrightarrow CH_2^* + OH^*$	1.00×10^{11}	20.2	17.7	1.00×10^{11}	12.5	3.1
15	$CH^* + OH^* \leftrightarrow CH_2^* + O^*$	1.00×10^{11}	19.3	13.2	1.00×10^{11}	19.9	20.5
16	$C^* + OH^* \leftrightarrow CH^* + O^*$	1.00×10^{11}	45.9	38.2	1.00×10^{11}	1.5	1.5
17	$CH_2^* + H_2O^* \leftrightarrow CH_3^* + OH^*$	1.00×10^{11}	5.1	19.5	1.00×10^{11}	18.6	0.0
18	$CH^* + H_2O^* \leftrightarrow CH_2^* + OH^*$	1.00×10^{11}	13.2	26.7	1.00×10^{11}	19.5	0.0
19	$C^* + H_2O^* \leftrightarrow CH^* + OH^*$	1.00×10^{11}	38.1	70.9	1.00×10^{11}	0.1	0.0
20	$CO^* + * \leftrightarrow C^* + O^*$	1.00×10^{11}	53.0	74.2	1.00×10^{11}	4.3	0.0
21	$CO_2^* + * \leftrightarrow CO^* + O^*$	1.00×10^{11}	21.2	43.1	1.00×10^{11}	3.6	0.0
22	$CO + * \leftrightarrow CO^*$	1.00	0.0	0.0	1.00×10^{13}	34.0	34.0
		0.71 [c]			1.21×10^{13} [c]		
23	$CO_2 + * \leftrightarrow CO_2^*$	1.00	0.0	0.0	1.00×10^{13}	17.0	17.0
		0.70 [c]			1.46×10^{12} [c]		
24	$CO_2^* + H^* \leftrightarrow CO^* + OH^*$	1.00×10^{11}	13.6	38.2	1.00×10^{11}	8.4	0.0
25	$CO^* + H^* \leftrightarrow CH^* + O^*$	1.00×10^{11}	80.5	106.0	1.00×10^{11}	0.0	0.0
26	$CO^* + H^* \leftrightarrow C^* + OH^*$	1.00×10^{11}	40.3	69.2	1.00×10^{11}	4.0	0.0
27	$CH_3 + * \leftrightarrow CH_3^*$	1.00	0.0	0.0	1.00×10^{13}	38.0	38.0
28	$CH_2 + * \leftrightarrow CH_2^*$	1.00	0.0	0.0	1.00×10^{13}	68.0	68.0
29	$CH + * \leftrightarrow CH^*$	1.00	0.0	0.0	1.00×10^{13}	97.0	97.0
30	$C + * \leftrightarrow C^*$	1.00	0.0	0.0	1.00×10^{13}	150.0	150.0
31	$2CO^* \leftrightarrow C^* + CO_2^*$	1.00×10^{11}	31.0	31.0	1.00×10^{11}	0.0	0.0
		2.40×10^{12} [c]			4.17×10^{09} [c]		

The activation energies are in kcal/mol, calculated at vacancy and oxygen dominated conditions. Preexponential values for each reaction in the first row of a reaction correspond to the screening mechanism whereas those in the second row (when one exists) are for the rigorously optimized parameters using the fluidized bed data (see relevant section).

[a] Screening mechanism with approximately optimized parameters to predict ignition and extinction temperatures as inlet methane composition is varied.
[b] Screening mechanism with approximately optimized parameters to predict methane conversion and syngas selectivity as temperature is varied.
[c] Rigorously optimized parameters to predict methane conversion and syngas selectivity as temperature is varied.

Table 3
Comparison of activation energies in kcal/mol of methane dissociation paths on Pt, Rh, and Ni

	Pt	Rh	Ni	
(1) $CH_3^* + {}^* = CH_2^* + H^*$	25.8			This work
	24.4	23.9	23.2	[46]
	25.7		23.9	[42]
(2) $CH_3^* + O^* = CH_2^* + OH^*$	20.2			This work
	17.9	21.1	25.1	[46]
	15.3		22.1	[42]
(3) $CH_2^* + {}^* = CH^* + H^*$	25.0			This work
	24.4	23.9	23.2	[46]
	24.3		23.2	[42]
(4) $CH_2^* + O^* = CH^* + OH^*$	19.9			This work
	16.5	20.9	25.1	[46]
	16.5		25.3	[42]
(5) $CH^* + {}^* = C^* + H^*$	5.4			This work
	5.4	4.9	4.5	[46]
	5.0		4.5	[42]
(6) $CH^* + O^* = C^* + OH^*$	1.5			This work
	0.0	2.6	7.3	[46]
	0.0		9.6	[42]

mixture of CH_4, O_2, and diluent N_2 was flowed in. A sharper drop in temperature was observed compared to experiments without O_2 addition. In fact, further increase in the O_2/CH_4 ratio led to an even bigger temperature drop. Despite these mixtures being dilute and fuel-rich ($CH_4/(CH_4 + O_2) > 0.8$, the complete combustion, being exothermic, should have led to a further increase of surface temperature. The unexpected results of Fig 7 tacitly indicate the enhancement of CH_4 decomposition due to the presence of O_2. This behavior is in qualitative agreement with the energetics, suggesting that CH_4 decomposition is faster in the presence of oxygen.

Au et al. calculated, using BOC and DFT, that when surface oxygen is on top of metal sites, it promotes methane dehydrogenation [51]. In contrast, oxygen at hollow metal sites does not promote dehydrogenation. It has been speculated that this occurs because hydrogen binds more strongly to surface oxygen (on top) than with the bare metal.

From the above results, there is evidence for the influence of oxygen on the dissociation of methane on the catalyst surface. Overall, theoretical calculations and some of the experiments point toward an enhancement of methane dissociation in the presence of oxygen, at moderate to high temperatures.

3.3. Energetics of the hydrogen-abstraction steps

The activation energies for the dehydrogenation of various adsorbed hydrocarbon species on Pt have recently been compiled [52]. These numbers have been found to be proportional to the C–H bond dissociation energy, being higher for sp^2-hybridized carbon species than for sp^3-hybridized ones. For methane dissociation, an activation energy of

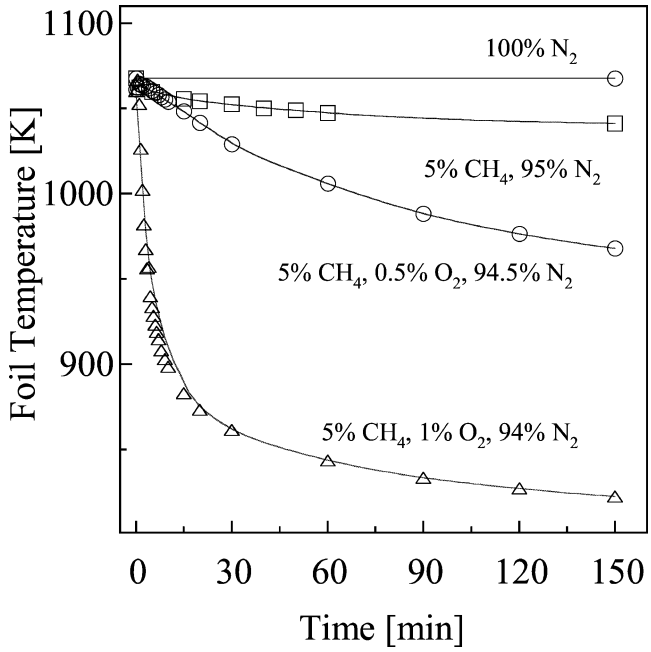

Fig. 7. Measured Pt foil temperature as a function of time for different reactant mixtures. A pressure of 1 atm, a flow velocity of 2.5 cm/s, and 25 amps input current are used. Addition of a small amount of oxygen in the feed facilitates carbon formation on the surface, which in turn leads to a reduction in the foil temperature, indicative of a possible reaction path involving oxygen-assisted methane dissociation on the Pt surface. The lines are just a guide to the eye.

18.4 kcal/mol has been observed in molecular beam experiments [53]

$$CH_4^* \rightarrow CH_3^* + H^*.$$

Our input heats of adsorption would yield a calculated value of 18 kcal/mol for this reaction, in good agreement with above. However, we do not explicitly include this reaction in our reaction scheme, using instead $CH_4 \rightarrow CH_3^* + H^*$ (direct dissociative adsorption of methane to methyl and hydrogen on the surface).

Temperature-programmed reaction has also been used to investigate the hydrogenation of methyl radicals on Pt(111) at UHV conditions using methyl bromide and hydrogen [54]. First, the TPD spectrum from methane adsorption has been used to derive an activation energy of 5 kcal/mol for

$$CH_4^* \rightarrow CH_4(\text{gas}).$$

We use 6 kcal/mol for this reaction as an input to our mechanism although we do not explicitly include this reaction (the heats of adsorptions of all species that participate in the surface mechanism are needed as an input to UBI-QEP, although we may further assume that species such as H_2^* and CH_4^* are too prone to dissociate on the surface, and may hence be left out of the surface-species set).

Second, methyl radical hydrogenation has been studied by simultaneous exposure to methyl bromide and hydrogen (with excess hydrogen). Through isotope-labeling studies and analysis of angular distributions of desorbed methane,

it has been confirmed that the rate constant derived can be assumed to be, for the elementary reaction of hydrogenation of $CH_3{}^*$ to CH_4,

$$CH_3{}^* + H^* \rightarrow CH_4(\text{gas}).$$

An activation energy of 8.8 kcal/mol has been derived for this reaction that is close (within the accuracy of the UBI-QEP method) to the 5.5 kcal/mol obtained in our calculations (Table 2).

4. A screening methane surface reaction mechanism

Using the mechanism listed in Table 2, predictions of experimental data may be obtained. Furthermore, improvements in the agreement of the model calculations with the experiments may be achieved through an optimization of the important prefactors, i.e., preexponentials and sticking coefficients. In this paper, we do a minimal amount of adjustment of the prefactors, choosing to leave the mechanism at the initial values whenever possible, as long as good agreement with a large set of experiments is obtained. The experiments used to optimize the mechanism against are the catalyst ignition (over the whole composition regime) and extinction (in the fuel-rich regime) temperatures of methane/air mixture over a foil vs inlet composition and the conversion of methane and selectivity to syngas vs temperature at 29.5% inlet CH_4–air in a fluidized bed reactor. The former type of experiment is crucial for start-up of all processes and safety considerations. The latter type of data is important in economics of partial oxidation or pollution abatement in complete combustion. The adjusted pre-exponentials/sticking coefficients are indicated in Table 2. A rigorous optimization of the preexponentials is touched upon at the end of the paper, with the mechanism obtained here meant to serve as a starting point for future work on mechanism optimization.

In terms of the modeling approach, the mean field assumption (spatially uniform distribution of adsorbates) is considered in all reactor models here as it is typically done in the literature. However, the BOC framework can also be impeded into Monte Carlo or multiscale reactor simulations [55]. The necessity to model the surface at the microscopic level (e.g., by using kinetic Monte Carlo simulations) under realistic conditions has been addressed in [56,57], where it was found that mean-field models are excellent for developing screening mechanisms. In this paper we mainly focus on modeling of a stagnation flow reactor and a continuous stirred tank reactor (CSTR). Instead of applying any simplifying assumptions, such as partial equilibrium or a quasi-steady-state hypothesis, the complete surface reaction mechanism is numerically solved in each case (microkinetics approach [40]). Details about the stagnation flow governing equations can be found in [26]. Modeling of an isothermal CSTR [58] simply involves steady state algebraic mass balance equations for the gas phase as well as the surface species, which are solved using Newton's method.

Figure 2 shows the prediction of ignition and extinction temperatures obtained using the stagnation-point flow reactor model (lines) [26], with our surface reaction mechanism coupled with detailed gas-phase chemistry (GRI 1.2 [41]). The ignition and extinction temperatures and the fuel-lean and fuel-rich composition limits of multiple steady states are fairly well predicted. The autothermal, i.e., self-sustained oxidation, compositional regime is overpredicted compared to the experimental data. A possible reason for this could be the presence of carbon on the catalyst surface at these conditions, which leads to high radiant efficiency. Simulations with higher heat losses have revealed that the autothermal regime vanishes completely. The catalyst surface is covered by O^* prior to the catalyst ignition, since oxygen can adsorb faster on Pt than methane. At ignition, O^* starts coming off the surface, freeing up sites for adsorption of methane, which are necessary for surface reactions. This feature has also been observed using other methane oxidation mechanisms, e.g., [12]. The competitive adsorption of methane and oxygen on the catalyst sites [12,15] is believed to drive ignition of these systems. The promotion effect of the fuel on ignition temperature (i.e., the fall in the ignition temperature with an increase in the fraction of fuel in the inlet) is also attributable to the competitive adsorption of methane and oxygen adsorption on Pt.

Figure 3b shows the predicted methane conversion and selectivity to syngas for 29.5% (fuel-rich) CH_4/air compared to fluidized bed experimental data [31]. Experimentally measured temperatures have been input into the model. We have chosen a CSTR-reactor model, with an area to volume ratio of 1.5×10^4 cm^{-1} and a typical residence time of 0.18 s (note that this varies slightly in experiments with operating conditions), to simulate these experiments. Based on the high conversions and low superficial velocity in these fluidized bed experiments [31], the ideal stirred tank may be a reasonable starting model (see [59] for a comparison between fluidized bed data and ideal stirred tank predictions for fuel conversion vs superficial velocity and [60] for a similar model in partial oxidation of methane on Ni/Al_2O_3), but the assumption is worth of further investigation. Finally, the Weisz criterion has been applied to this system. Assuming that the adsorption of methane is rate-determining, it has been found that internal mass transport limitations may be ignored in this case.

Good agreement between the experiments and the simulations is seen, despite the ideality of the reactor-scale model chosen here. Some discrepancies (for example, the drop in CO selectivity at lower temperatures) indicate the potential for improving the reactor-scale model and/or the surface reaction mechanism. We consider this topic below. It will be shown in a later section that this set of data is more influenced by the surface chemistry than the ignition data.

5. Validation of the screening surface reaction mechanism

In this section, we validate the new surface reaction mechanism with additional experiments to ensure that gross features are correctly predicted. Some of these comparisons are semiquantitative in nature, since specifics of reactor geometry and transport phenomena need to be carefully taken into account for quantitative comparison to each experiment. This will be the subject of a forthcoming publication. No adjustment of the preexponentials/sticking coefficients is resorted to in this section.

5.1. Ignition temperatures of diluted methane/oxygen mixtures

The effect of dilution on the ignition temperatures is important to study to delineate thermal versus kinetic effects (see discussion above in section on experimental data). In order to compare with foil experiments, we have performed simulations here, using the stagnation-point flow geometry code [26] and the screening surface reaction mechanism of Table 2 for 94% N_2-dilution, at various inlet CH_4/O_2 ratios. The parameters of the simulations are given in the caption. Figure 1 summarizes predictions of ignition temperatures for such nitrogen-diluted methane–oxygen mixtures. Good agreement with the ignition temperatures from various groups is found. The lack of significant dependence of the ignition temperature on dilution (at a fixed $CH_4/(CH_4 + O_2)$ ratio), which is in agreement with experimental data, indicates the predominance of surface kinetic effects on catalytic ignition.

5.2. Dependence of methane conversion and selectivity to syngas on inlet composition for fuel-rich mixtures

In the previous section, we have examined the predictions of methane conversion and syngas selectivity at a fixed inlet methane composition, as a function of temperature. The effect of inlet fuel composition is important both for validation of the mechanism and for potential optimization with respect to operating conditions. We have again chosen to compare with fluidized bed data [31], using the same model as above.

Figure 3 (top) shows experimental data and model predictions of methane conversion and syngas selectivity versus inlet methane composition. The reactor temperature has been fixed at the corresponding measured outlet temperature, for these predictions. Good agreement of predictions with experiments is observed in this case as well. Experiments conducted in monoliths [3] could be simulated using more sophisticated, two-dimensional reactor scale models coupled with this surface reaction mechanism. Such detailed two-dimensional CFD calculations are slowly emerging [17,36, 37,61] and could be used for parameter optimization, starting from the screening mechanism proposed here.

5.3. Bifurcation characteristics and LIF–OH concentration for fuel-lean methane/air mixtures

In recent modeling studies, a homogeneous one-dimensional axial reactor with convection and diffusion has been used and found to give good agreement with experiments over Ni catalyst [38]. However, it has been concluded that in the case of Pt-gauzes, proper inclusion of surface chemistry is essential to predict experimental trends [38]. Next, we compare our predictions of bifurcation and OH mole fractions at fuel-lean conditions with their experimental data for Pt gauzes [38] summarized in Fig 5. The stagnation-point geometry code is again utilized in combination with detailed gas-phase chemistry and the surface reaction mechanism of this work. These comparisons are meant to be merely qualitative in this case.

Figure 6 shows one-parameter continuation curves, with the surface temperature and surface OH mole fraction as a function of the inlet power supplied to the surface, at two different fuel-lean inlet methane compositions. The simulations' parameters are given in the caption. In the case of the 3.25% CH_4/air mixture, no turning points (ignition and extinction) are found. The OH mole fraction next to the surface monotonically increases as the input power is raised, consistent with data depicted in Fig. 5a. On the other hand, when the inlet methane composition is increased to 4.5%, both catalytic (lower temperature) and homogeneous (higher temperature) ignition and extinction are seen. The catalytic ignition temperature is in good agreement with experimental data [38]. A maximum in the OH mole fraction as a function of the input power to the surface is also in agreement with experimental data shown in Fig 5. The inset in Fig. 6 shows the OH mole fraction profiles obtained in our simulations, at various inlet methane compositions and for a surface temperature of 1400 K. Both features, the maximum in the OH mole fraction slightly away from the surface and the increase in OH mole fraction throughout the boundary layer with increasing inlet methane composition, are consistent with experimental observations. Better quantitative comparison between experiments and simulations (e.g., regarding the thickness of the OH mole fraction boundary layer) could probably be achieved by choosing a more appropriate reactor-scale model for the gauze experiments. Since the overall experimental features are well captured, we leave this for future work. It appears that for both compositions a noticeable fraction of OH near the surface is observed only upon ignition of the gas-phase chemistry. This observation indicates that under the conditions of our study, Pt serves as a sink rather than a source of OH radicals upon gas-phase ignition.

5.4. Methane conversion and selectivity to CO for fuel-lean methane/air mixtures

The fuel conversion and CO selectivity data from Pt foil reactors [33] are examined in this section. These experi-

ments span a large regime of surface temperatures (400–1650 K) and are important indicators of issues such as catalytic reactivity, homogeneous ignition temperature, and the coupling between homogeneous and catalytic chemistries. We have performed simulations using the stagnation-point flow geometry code and the surface reaction mechanism of this article. The conversion of methane is calculated following the modeling work of Dupont et al., fixing an expansion factor K value in order that simulations agree with experiments at ~ 1200 K (see [33] for more discussion). The K factor of 0.07 suggested by Dupont et al. led to good agreement with our experiments but to underprediction of the data by Dupont et al. A factor of $K = 0.14$ has been used for the latter. Both simulations are indicated with lines in Fig. 4. The experimental homogeneous ignition temperature (seen as a jump in the methane conversion at ~ 1600 K) is also well captured in our simulations. A comparison between the predicted CO selectivity and the experimental data of Dupont et al. was also performed, and reasonable agreement was obtained, as shown in bottom of Fig. 4.

6. Sensitivity and reaction path analyses

The predictions of the surface reaction mechanism developed here may further be analyzed in order to determine the controlling reactions in each case. This is achieved by a combination of reaction path and sensitivity analyses. The former involves the determination of the main reactions participating in the formation and destruction of the different surface species, whereas the latter entails the calculation of the change in a predicted quantity when a specific preexponential is reduced by 10%.

6.1. Bifurcation features in a stagnation reactor

Catalytic ignition of methane has been modeled extensively in the past (see [12,15,62,63]). Sensitivity analysis results obtained here for ignition temperatures at 10 and 80% inlet methane/air are shown in Fig. 8. These results are consistent with previously published results. In summary, over the whole range of inlet compositions, ignition temperature is mainly governed by the adsorption of methane and oxygen and the desorption of O*. A very small dependence on the oxygen-assisted decomposition of methyl is also observed.

Next, reaction path analysis is performed for the 10% inlet methane case prior to ignition (~ 800 K) and extinction (~ 1000 K) (see Fig. 9). The corresponding surface coverages at these conditions are also indicated. While the paths for formation of CO* (from the oxidation of C* and CH* by O*) and CO_2* (from the oxidation of CO* by O*) remain the same at these two conditions, the paths for the dissociation of methane to carbon on the surface are different. At ignition, the oxygen and hydroxyl-assisted pathways for methane decomposition to methyl dominate over the pyrolytic one, whereas under extinction conditions, where

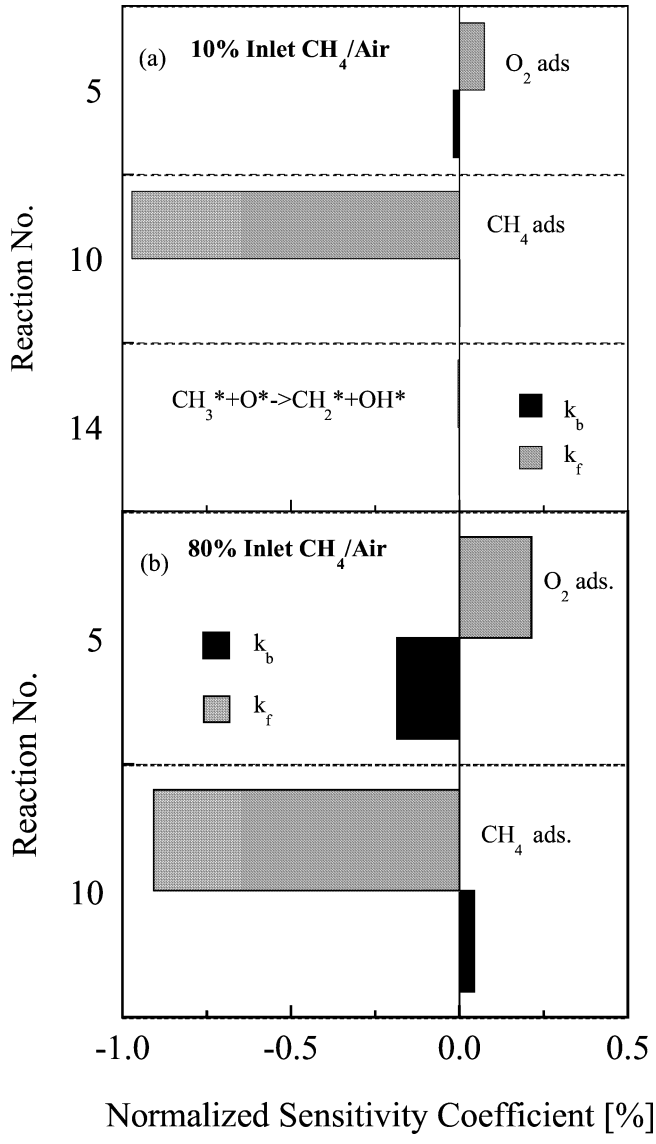

Fig. 8. Sensitivity analysis obtained for ignition temperatures at 10 and 80% inlet CH_4–air for 10% reduction in reaction prefactors (preexponentials or sticking coefficients). The normalized sensitivity coefficient is defined as the ratio of the relative change in ignition temperature and the relative change in prefactors. The reaction numbers correspond to the ones in Table 2. Adsorption of methane and oxygen and desorption of O* control ignition temperatures.

higher temperatures and lower O* coverage occur, the pyrolytic pathway takes over.

We believe that this behavior is caused by the change in activation energies of the oxygen-assisted steps with increase in O* coverage (see section above on Methane Dissociation Steps), the competition for O* by different paths in the mechanism, and the change in temperature. For example, if we assumed that all the O* on the surface at these two conditions were available for the dissociation of methane to methyl, we would obtain a rate of pyrolytic methane dissociation about half that of the oxygen-assisted rate at 800 K. This is consistent with the reaction path analysis (RPA) shown in top of Fig. 9. However, at 1000 K the rate

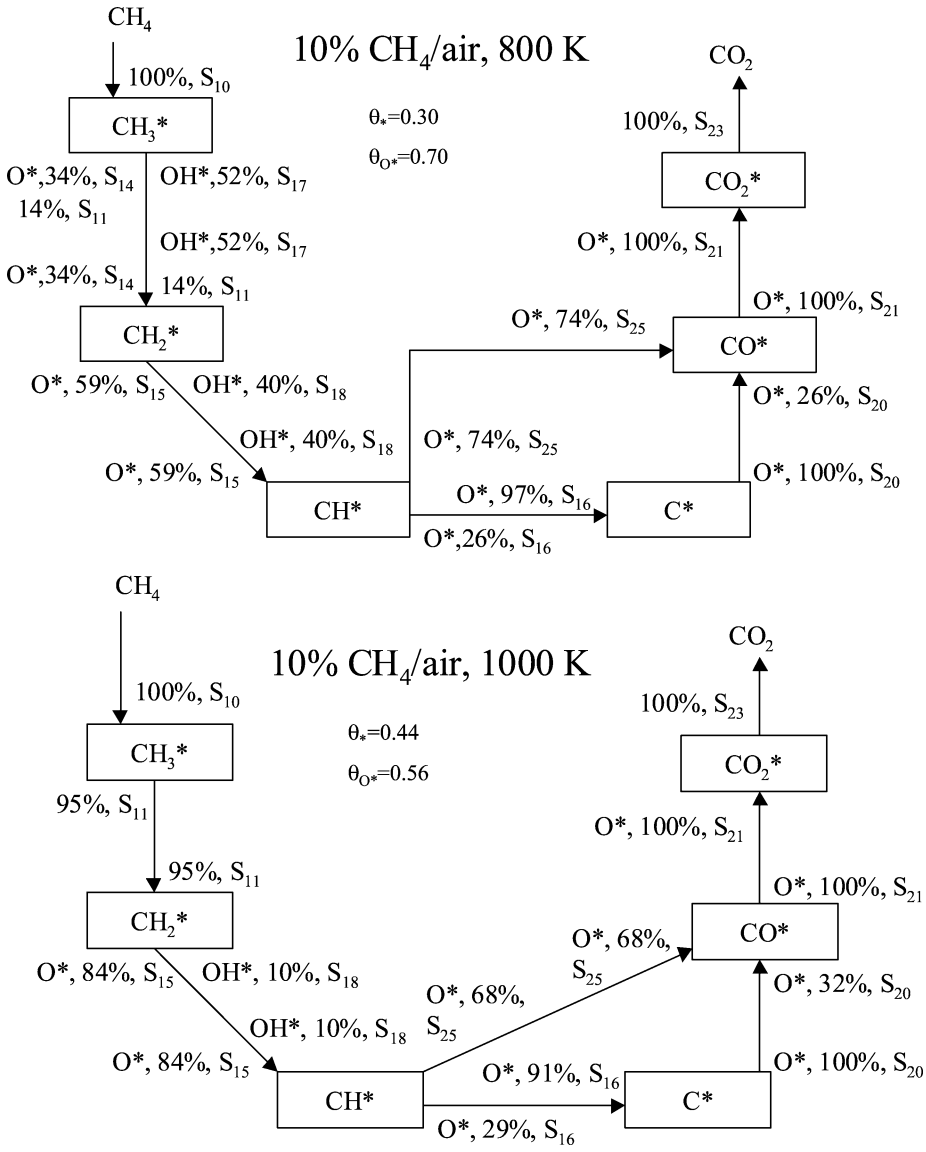

Fig. 9. Reaction path analysis for a 10% CH_4/air mixture, close to ignition (top) and extinction (bottom). Large surface coverages of various species are also indicated. The surface species are represented in boxes. Arrows to and from the box indicate paths producing and consuming the species, respectively. In the text next to the arrows, S_i indicates the ith surface reaction (from Table 2), X^* indicates additional surface species involved in the reaction, and Y% indicates the percentage contribution of the particular reaction to the net production/consumption rate of the involved species. Close to ignition, oxygen-assisted paths are dominant in the dissociation of methane, whereas close to extinction, the pyrolytic path for dissociation of methyl to methylene becomes important.

of pyrolytic dissociation would be about 1.5 times that of the oxygen-assisted step, which is also consistent with the RPA shown in bottom of Fig. 9. Furthermore, some effects are attributable to the fact that O^* is preferentially consumed in other parts of the mechanism at these temperature conditions. In particular, the dissociation of CH_2^* to CH^* prefers the oxygen-assisted path more at 1000 K than at 800 K.

Finally, reaction path analysis for fuel-lean mixtures at high temperatures has revealed that OH^* formation occurs both directly from oxidation of H^* on the surface and from the oxidation of various hydrocarbons. This points toward a coupling of the C/O and H/O chemistries on the catalyst surface. LIF measurements of OH (such as the ones shown in a previous section) do therefore form relevant data sets for optimization/validation of methane catalytic oxidation mechanisms.

6.2. Methane conversion and syngas selectivity

Figure 10 shows the sensitivity analysis for methane conversion and syngas selectivity in CSTR simulations at 29.5% inlet methane/air at a surface temperature of 1123 K, whereas Fig. 11 shows the sensitivity analysis for methane conversion, performed for stagnation reactor simulations at 6% inlet methane/air at a surface temperature of 1400 K.

In the former case, a very strong dependence on methane adsorption is observed. At these temperatures, the surface reactions are sufficiently fast that they do not significantly

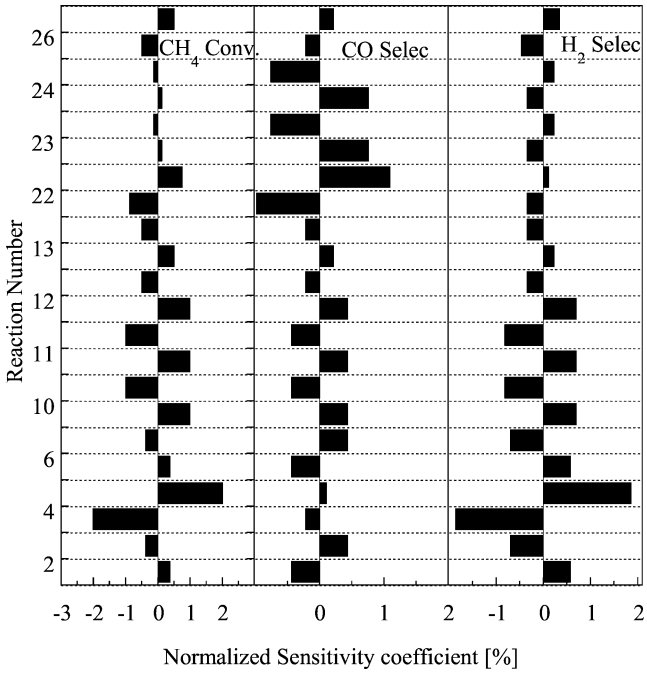

Fig. 10. Sensitivity analysis for methane conversion and CO and H_2 selectivities, at 29.5% CH_4/air and 1123 K in CSTR simulations. For each reaction number, the lower bar is for the forward reaction and the higher one for the backward reaction. The normalized sensitivity coefficient is defined as in Fig. 8. For these fuel-rich mixtures at moderate temperatures, apart from the adsorption of CH_4, CO, and H_2, the pyrolytic methane dissociation steps affect conversion and selectivity.

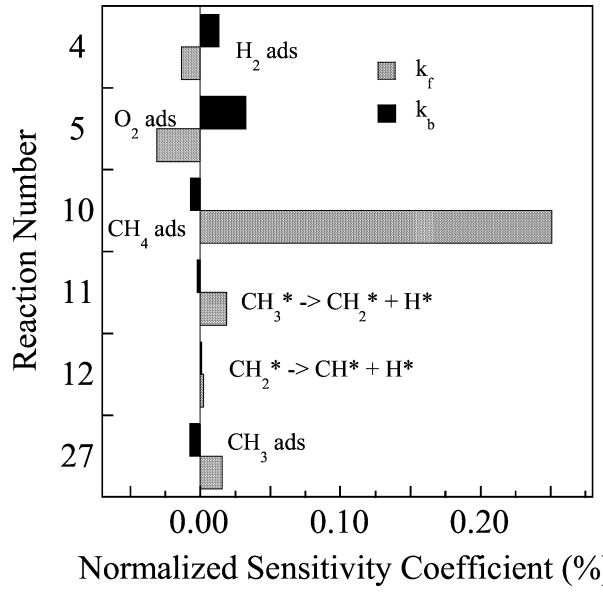

Fig. 11. Sensitivity analysis for methane conversion at 6% CH_4/air and 1400 K in stagnation reactor flow simulations. The normalized sensitivity coefficient is defined as in Fig. 8. At these elevated temperatures for fuel-lean mixtures, adsorption of methane is the most important step.

affect the conversion of methane. Thus, a proper description of methane adsorption is crucial for accurate prediction of methane conversion (see predictions in the previous section, in Fig. 3).

For the fuel-rich mixtures, sensitivity analysis (Fig. 10) reveals that the methane conversion is affected by methane adsorption, pyrolytic methane dissociation paths, H_2 adsorption, and to a less extent by CO adsorption. The selectivity to CO is strongly dependent on CO and CO_2 adsorption/desorption steps, methane adsorption and decomposition, and the oxidation of CO^* to $CO_2{}^*$ by OH^*. The selectivity to H_2 on the other hand is affected by H_2 adsorption/desorption, methane adsorption and decomposition, and the formation of H_2O from H and OH. Some interesting facts to note are that apart from the adsorption/desorption steps, the pyrolytic paths of methane decomposition, and certain surface reactions of CO^* and H^* are important for the prediction of syngas selectivities, and to a less extent for methane conversion. This demonstrates that these experimental results are a good target for optimization of the new surface reaction mechanism.

Further analysis of a fuel-lean mixture (5%) at 1123 K in CSTR simulations (results not shown) has revealed that methane conversion (which is ~ 1.0 at those conditions) is insensitive to all the reaction steps. The selectivity to CO depends on O_2, CO, and CO_2 adsorption/desorption steps, and the oxidation of CO^* to $CO_2{}^*$. Similarly, the selectivity to H_2 depends on O_2, H_2, and H_2O adsorption/desorption steps, and the reaction steps for formation of H_2O. Thus, the difference between fuel-lean and fuel-rich mixtures as far as the selectivities to CO and H_2 are concerned, when the temperature (and the reactor model) are the same, is that the former depend on the adsorption/desorption of oxygen whereas the latter depend on the adsorption/desorption of methane.

Reaction path analysis for the 29.5% inlet methane case (CSTR simulations) reveals the importance of the pyrolytic path for the hydrogen abstraction from methyl. Complex interconversions of CO and CO_2 (through oxidation of CO^* to $CO_2{}^*$ by O^* and reduction of $CO_2{}^*$ to CO^* by C^*) are also seen.

7. Towards an optimized mechanism

Given that the predictions of the fluidized bed data are not very good (especially the effect of temperature on CO selectivity shown in bottom of Fig. 3), here we explore whether this is a result of lack of rigorous optimization of the methane surface reaction mechanism. To achieve this, we employ the solution mapping methodology outlined in [18] within a new iterative approach (to be discussed in detail elsewhere [65]), where polynomials get refined after each optimization iteration. The CH_4 conversion, CO selectivity, and H_2 selectivity data in the fluidized bed reactor serve as the targeted experiments. We optimize preexponential factors only, keeping activation energies unchanged due to higher confidence in DFT and BOC calculations.

In the local sensitivity analysis, it is found that the methane conversion is primarily affected by methane ad-

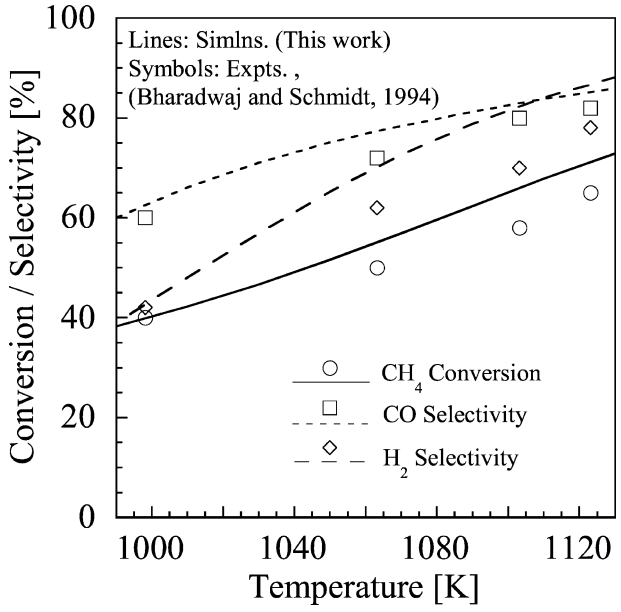

Fig. 12. Rigorous optimization of parameters using the screening mechanism of Table 2 and the fluidized bed reactor data on methane conversion and syngas selectivity as targeted experiments [31]. An iterative optimization approach enables to predict these experimental data reasonably well. The optimized parameters are also listed in Table 2.

sorption and desorption as well as H_2 adsorption and desorption, and the CO selectivity depends primarily on CO adsorption and desorption as well as CO_2 adsorption and desorption, whereas H_2 selectivity is primarily sensitive to H_2 adsorption and desorption as well as H_2O adsorption and desorption steps. Polynomials are developed in each iteration for all three types of data as a function of these sensitive parameters, and finally the distance between experimental data and the polynomial predictions was minimized using simulated annealing. Fig. 12 shows the performance of the optimized mechanism. The CH_4 conversion and CO selectivity predictions are highly improved, whereas the H_2 selectivity predictions are improved only in the low temperature regime. The rigorously optimized parameters are presented in Table 2. It is seen that the performance of the mechanism can be improved with minimal adjustment of parameters. Future work should analyze simultaneously data for methane, hydrogen, carbon monoxide, and their mixtures in order to build the foundations for a fully optimized natural-gas-to-syngas reaction mechanism.

8. Conclusions

A comprehensive C1 mechanism for the oxidation of methane over Pt has been developed. Various surface paths for methane decomposition, including the pyrolytic and oxygen- and hydroxyl-assisted ones, have been employed. Thermodynamic consistency in energetics has been ensured by computing the reaction activation energies and heats as functions of the heats of adsorption of the species involved in the reaction mechanism, using the UBI-QEP framework. The initial preexponentials and sticking coefficient values were based on transition state theory (order of magnitude estimates) and the H_2/O_2 subset developed previously.

A host of experimental data for methane oxidation on Pt have been obtained from various literature sources and augmented by experiments conducted in our laboratory. Predictions of ignition and extinction temperatures at varying inlet compositions, LIF OH mole fraction profiles, and methane conversion and selectivity to CO and H_2 at different inlet compositions and catalyst temperatures have been obtained using the new surface reaction mechanism coupled with detailed gas-phase chemistry and various reactor scale models. While the experiments have been conducted on polycrystalline Pt (foil reactor data) or supported catalyst structures (fluidized bed data), the input to our methodology was mostly from work on Pt(111) (a dominant crystal face of Pt). Despite this "materials gap," reasonable agreement is observed over the range of conditions studied.

Reaction path and sensitivity analyses have then been conducted in order to determine the important reaction pathways at different conditions. The pyrolytic pathway for methane decomposition is seen to dominate under low-oxygen, high-temperature conditions, whereas the oxygen/hydroxyl-assisted pathways for methane decomposition prevail at preignition (low-temperature) conditions. A coupling between the carbon and hydrogen subsets of the mechanism has been found in predicting the OH mole fraction. Differences between fuel-lean and fuel-rich mixtures with respect to controlling reactions have been identified. The overall good performance of the mechanism in predicting a wide variety of experimental data demonstrates the potential of the proposed approach. Preliminary work on rigorous optimization of reaction steps shows the feasibility of optimizing large surface reaction mechanisms needed in large fuel conversion to syngas or hydrogen.

Acknowledgments

This article was prepared with the support of the US Department of Energy, under Award DE-FC26-00NT41027. However, any opinions, findings, conclusions, or recommendations expressed herein are those of the authors and do not necessarily reflect the views of the DOE.

References

[1] W.C. Pfefferle, L.D. Pfefferle, Prog. Energy Combust. Sci. 12 (1986) 25.
[2] R. Prasad, L.A. Kennedy, E. Ruckenstein, Catal. Rev. Sci. Eng. 26 (1984) 1.
[3] D.A. Hickman, L.D. Schmidt, Science 259 (1993) 343.
[4] K. Heitnes, S. Lindberg, O.A. Rokstad, A. Holmen, Catal. Today 24 (1995) 211.
[5] P. Aghalayam, Y.K. Park, D.G. Vlachos, Catalysis 15 (2000) 98.

[6] D.A. Goetsch, G.R. Say, J.M. Vargas, P.E. Eberly, United States Patent, Exxon Research and Engineering Company, United States, 1989.
[7] G.A. Foulds, J.A. Lapszewicz, Catalysis (1994) 413.
[8] S.C. Tsang, J.B. Claridge, M.L.H. Green, Catal. Today 23 (1995) 3.
[9] X. Song, W.R. Williams, L.D. Schmidt, R. Aris, Combust. Flame 84 (1991) 292.
[10] P. Markatou, L.D. Pfefferle, M.D. Smooke, Combust. Flame 93 (1993) 185.
[11] P.A. Bui, E.A. Wilder, D.G. Vlachos, P.R. Westmoreland, Combust. Sci. Technol. 129 (1–6) (1997) 243.
[12] P.-A. Bui, D.G. Vlachos, P.R. Westmoreland, Surf. Sci. 385 (2–3) (1997) L1029.
[13] D.A. Hickman, L.D. Schmidt, AIChE J. 39 (7) (1993) 1164.
[14] J. Frauhammer, G. Veser, Chem. Ing. Tech. 70 (8) (1998) 1020.
[15] O. Deutschmann, R. Schmidt, F. Behrendt, J. Warnatz, in: Twenty Sixth Symposium (International) on Combustion, The Combustion Institute, Pittsburgh, 1996, p. 1747.
[16] P. Aghalayam, Y.K. Park, D.G. Vlachos, in: Joint Combustion Meeting of the US Sections, The Combustion Institute, Washington, DC, 1999, p. 745.
[17] D.K. Zerkle, M.D. Allendorf, M. Wolf, O. Deutschmann, J. Catal. 196 (2000) 18.
[18] P. Aghalayam, Y.K. Park, D.G. Vlachos, AIChE J. 46 (10) (2000) 2017.
[19] Y.K. Park, P. Aghalayam, D.G. Vlachos, J. Phys. Chem. A 103 (40) (1999) 8101.
[20] P. Aghalayam, Y.K. Park, D.G. Vlachos, Symp. Int. Combustion 28 (2000) 1331.
[21] Y.K. Park, P.A. Bui, D.G. Vlachos, AIChE J. 44 (9) (1998) 2035.
[22] F. Behrendt, O. Deutschmann, R. Schmidt, J. Warnatz, in: Symposium in Catalysis, Heterogeneous Hydrocarbon Oxidation, Spring ACS Meeting, New Orleans, 1996, p. 48.
[23] T.A. Griffin, L.D. Pfefferle, AIChE J. 36 (1990) 861.
[24] G. Veser, L.D. Schmidt, AIChE J. 42 (4) (1996) 1077.
[25] Y.K. Park, Homogeneous and catalytic oxidation of hydrogen and methane, PhD thesis, Department of Chemical Engineering, University of Massachusetts, Amherst, 2000.
[26] P.A. Bui, D.G. Vlachos, P.R. Westmoreland, Ind. Eng. Chem. Res. 36 (7) (1997) 2558.
[27] M. Ziauddin, A. Balakrishna, D.G. Vlachos, L.D. Schmidt, Combust. Flame 110 (3) (1997) 377.
[28] Y.K. Park, D.G. Vlachos, Combust. Flame 114 (1–2) (1998) 214.
[29] N. Fernandes, Y.K. Park, D.G. Vlachos, Combust. Flame 118 (1–2) (1999) 164.
[30] W.R. Williams, M.T. Stenzel, X. Song, L.D. Schmidt, Combust. Flame 84 (1991) 277.
[31] S.S. Bharadwaj, L.D. Schmidt, J. Catal. 146 (1994) 11.
[32] D.L. Trimm, C.-W. Lam, Chem. Eng. Sci. 35 (1980) 1405.
[33] V. Dupont, S.-H. Zhang, A. Williams, Int. J. Energy Res. 24 (14) (2000) 1291.
[34] T.A. Griffin, M. Calabrese, L.D. Pfefferle, A. Sappey, R. Copend, D.R. Crosley, Combust. Flame 90 (1992) 11.
[35] J. Warnatz, M.D. Allendorf, R.J. Kee, M.E. Coltrin, Combust. Flame 96 (1994) 393.
[36] L.L. Raja, R.J. Kee, O. Deutschmann, J. Warnatz, L.D. Schmidt, Catal. Today 59 (1–2) (2000) 47.
[37] J. Mantzaras, C. Appel, P. Benz, J.W. Daily, J. Andrae, Proc. Combust. Inst. 28 (2000) 1349.
[38] M.B. Davis, M.D. Pawson, G. Veser, L.D. Schmidt, Combust. Flame 123 (1–2) (2000) 159.
[39] E. Shustorovich, H. Sellers, Surf. Sci. Rep. 31 (1998) 1.
[40] I.A. Dumesic, D.F. Rud, L.M. Aparicio, J.E. Rekoske, A.A. Revino, The Microkinetics of Heterogeneous Catalysis, American Chemical Society, Washington, DC, 1993.
[41] C.T. Bowman, R.K. Hanson, D.F. Davidson, W.C. Gardiner Jr., V. Lissianski, G.P. Smith, D.M. Golden, M. Frenklach, M.E. Goldenberg, available at http://www.me.berkeley.edu/gri_mech/new21/version12/text12.html.
[42] P.P. Olivera, E.M. Patrito, H. Sellers, Surf. Sci. 327 (1995) 330.
[43] Y. Ishikawa, M.-S. Liao, C.R. Cabrera, Surf. Sci. 463 (2000) 66.
[44] M.J. Hei, H.B. Chen, J. Yi, Y.J. Lin, G. Wei, D.W. Liao, Surf. Sci. 417 (1998) 82.
[45] E. Shustorovich, A.T. Bell, Surf. Sci. 248 (3) (1991) 359.
[46] A.V. Zeigarnik, R.E. Valdés-Pérez, J. Pesenti, J. Phys. Chem. B 104 (2000) 997.
[47] E.M. Patrito, P. Paredes Olivera, H. Sellers, Surf. Sci. 306 (1994) 447.
[48] C.T. Au, H.Y. Wang, J. Catal. 167 (1997) 337.
[49] Y.H. Hu, E. Ruckenstein, Catal. Lett. 34 (1995) 41.
[50] Y.H. Hu, E. Ruckenstein, J. Catal. 158 (1996) 260.
[51] C.-T. Au, C.-F. Ng, M.-S. Liao, J. Catal. 185 (1999) 12.
[52] C.T. Campbell, Y.-K. Sun, Chem. Phys. Lett. 179 (1,2) (1991) 53.
[53] Y.-K. Sun, W.H. Weinberg, J. Vac. Sci. Technol. A. 8 (3) (1990) 2445.
[54] V.A. Ukraintsev, I. Harrison, Surf. Sci. Lett. 286 (1993) L571.
[55] S. Raimondeau, D.G. Vlachos, Chem. Eng. J. (2002), in press.
[56] S. Raimondeau, D.G. Vlachos, Comput. Chem. Eng. 26 (7–8) (2002) 965.
[57] S. Raimondeau, D.G. Vlachos, Ind. Eng. Chem. Res., submitted for publication.
[58] P. Glarborg, R.J. Kee, J.F. Grcar, J.A. Miller, SANDIA National Laboratory Report, SAND86-8209, 1991.
[59] J.M. Smith, Chemical Engineering Kinetics, McGraw–Hill, New York, 1981.
[60] T. Wurzel, L. Mleczko, Chem. Eng. J. 69 (1998) 127.
[61] O. Deutschmann, L.D. Schmidt, AIChE J. 44 (11) (1998) 2465.
[62] C. Trevino, AIChE J. 45 (3) (1999) 567.
[63] P. Aghalayam, D.G. Vlachos, in: Eastern States Combustion Symposium, Raleigh, NC, 1999, p. 217.
[64] E. Shustorovich, in: D.D. Eley, H. Pines, P.B. Weisz (Eds.), Advances in Catalysis, Academic Press, San Diego, CA, 1990, p. 101.
[65] S.G. Davis, A.B. Mhadeshwar, D.G. Vlachos, H. Wang, Int. J. Chem. Kinet., submitted for publication.